Article

Cell Reports

TIA-1 Self-Multimerization, Phase Separation, and Recruitment into Stress Granules Are Dynamically Regulated by Zn^{2+}

Graphical Abstract

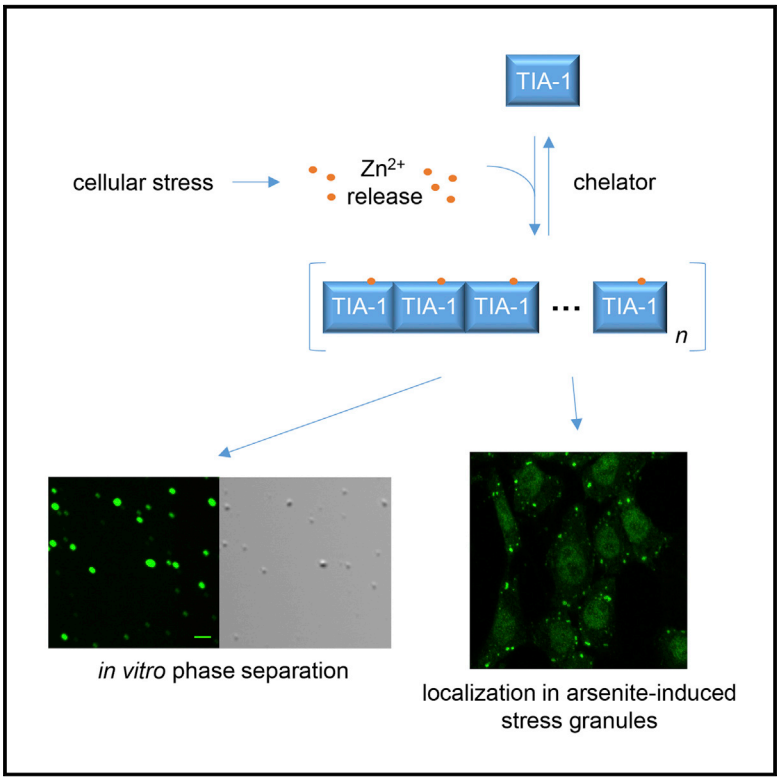

Highlights

- Zn^{2+} is released during arsenite-induced oxidative stress
- Zn^{2+} causes rapid and reversible self-multimerization and phase separation of TIA-1
- Zn^{2+} is important for recruitment of TIA-1 into stress granules, as well as retention
- Zn^{2+} stimulates the effects of arsenite on formation of TIA-1-positive stress granules

Authors

Joseph B. Rayman, Kevin A. Karl, Eric R. Kandel

Correspondence

erk5@columbia.edu

In Brief

Rayman et al. show that Zn^{2+} is a stress-inducible second messenger that triggers self-multimerization and phase separation of TIA-1 and regulates dynamic recruitment of TIA-1 into stress granules. This mechanism is part of an adaptive cellular response to environmental adversity.

Rayman et al., 2018, Cell Reports *22*, 59–71
January 2, 2018
https://doi.org/10.1016/j.celrep.2017.12.036

CellPress

Cell Reports
Article

TIA-1 Self-Multimerization, Phase Separation, and Recruitment into Stress Granules Are Dynamically Regulated by Zn^{2+}

Joseph B. Rayman,[1,4] Kevin A. Karl,[1,3,4] and Eric R. Kandel[1,2,3,4,5,6,*]
[1]Department of Neuroscience, College of Physicians and Surgeons of Columbia University, New York, NY 10032, USA
[2]Department of Psychiatry, College of Physicians and Surgeons of Columbia University, New York, NY 10032, USA
[3]Howard Hughes Medical Institute at Columbia University, New York, NY 10032, USA
[4]Zuckerman Mind Brain Behavior Institute, Columbia University, New York, NY 10032, USA
[5]Kavli Institute for Brain Science, Columbia University, New York, NY 10032, USA
[6]Lead Contact
*Correspondence: erk5@columbia.edu
https://doi.org/10.1016/j.celrep.2017.12.036

SUMMARY

Stress granules are non-membranous structures that transiently form in the cytoplasm during cellular stress, where they promote translational repression of non-essential RNAs and modulate cell signaling by sequestering key signal transduction proteins. These and other functions of stress granules facilitate an adaptive cellular response to environmental adversity. A key component of stress granules is the prion-related RNA-binding protein, T cell intracellular antigen-1 (TIA-1). Here, we report that recombinant TIA-1 undergoes rapid multimerization and phase separation in the presence of divalent zinc, which can be reversed by the zinc chelator, TPEN. Similarly, the formation and maintenance of TIA-1-positive stress granules in arsenite-treated cells are inhibited by TPEN. In addition, Zn^{2+} is released in cells treated with arsenite, before stress granule formation. These findings suggest that Zn^{2+} is a physiological ligand of TIA-1, acting as a stress-inducible second messenger to promote multimerization of TIA-1 and subsequent localization into stress granules.

INTRODUCTION

Stress granules are cytoplasmic foci that assemble when cells are exposed to environmental adversity, such as oxidative stress, viral infection, and extremes of pH or temperature (Kedersha et al., 2013). During cellular stress, non-essential mRNAs are recruited into stress granules in the form of abortive pre-initiation complexes, while mRNAs encoding heat shock proteins and other essential factors are excluded (Kedersha et al., 2013). By selectively maintaining a subset of cellular mRNAs in a translationally repressed state, stress granules enable the efficient reallocation of cellular resources toward adaptive reprogramming of the proteome (Anderson and Kedersha, 2008; Buchan and Parker, 2009). In addition, stress granules alter the flow of cellular information by sequestering proteins involved in signal transduction (Arimoto et al., 2008; Kedersha et al., 2013; Wippich et al., 2013). Thus, stress granules serve an important protective function in eukaryotes in the face of environmental challenge.

A growing body of evidence suggests that stress granules are more precisely described as liquid droplets formed by phase separation in the cytoplasm. Stress granules are enriched in proteins containing intrinsically disordered regions (IDRs), which have been found to aggregate spontaneously *in vitro* (Dyson and Wright, 2005). Furthermore, these aggregates exhibit properties of liquids or hydrogels and can likewise undergo mechanical shearing and demixing (Kato et al., 2012; Protter and Parker, 2016). In addition, the resident half-life of some stress granule components is on the order of seconds (Buchan and Parker, 2009; Kedersha et al., 2000). Finally, studies point to a nuanced view in which stress granules contain a stable, electron-dense core region that is less dynamic than the shell layer (Jain et al., 2016). Thus, stress granules are not homogeneous, static structures with defined stoichiometry but rather highly dynamic entities that are poised to respond to prevailing environmental conditions.

One of the canonical proteins found in stress granules is T cell intracellular antigen-1 (TIA-1), a prion-related RNA binding protein that harbors an intrinsically disordered prion-related domain at its C terminus. Overexpression of the prion-related domain alone blocks the formation of stress granules in a dominant-negative manner, while overexpression of full-length TIA-1 is sufficient to cause the formation of stress granules in the absence of stress (Gilks et al., 2004; Kedersha and Anderson, 2007). Although progress has been made in the development of experimental and computational models for stress granule formation (Kedersha et al., 2008; Ohshima et al., 2015; Protter and Parker, 2016), it is unclear how changes in the structural state of TIA-1 are coupled to relevant signaling pathways to trigger their assembly.

The identification of small molecules that specifically target TIA-1 aggregation could reveal useful tools with which to explore the structure and function of TIA-1. To this end, we developed a Förster resonance energy transfer (FRET) assay using enhanced cyan fluorescent protein (ECFP)-tagged and enhanced yellow fluorescent protein (EYFP)-tagged TIA-1 to screen for

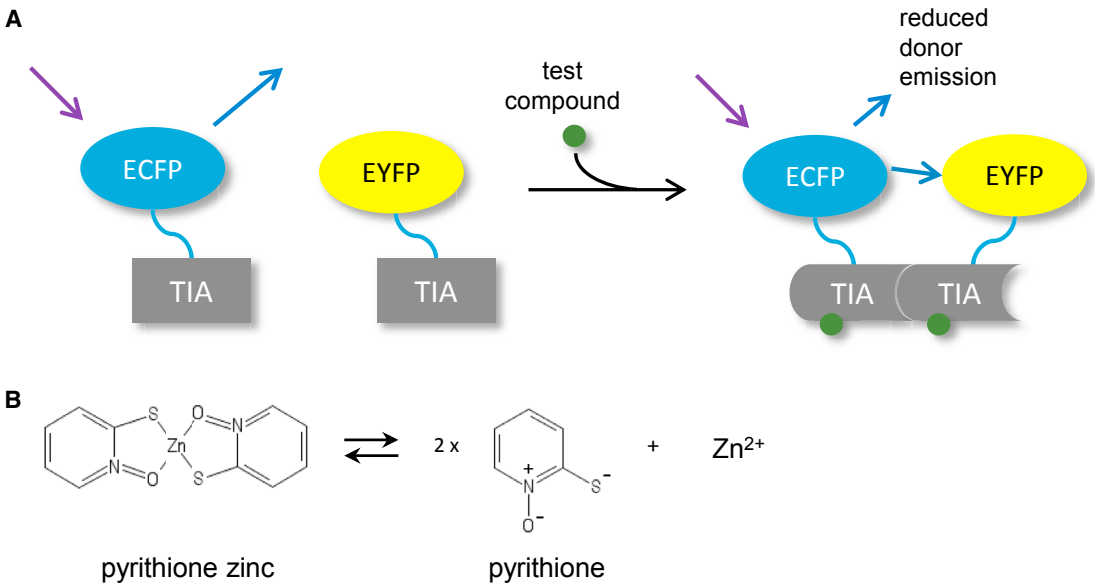

Figure 1. FRET-Based Screen to Identify Compounds that Promote TIA-1 Self-Multimerization

(A) Schematic of FRET assay.

(B) Pyrithion zinc (PZ), a compound identified in the screen, exists in equilibrium with pyrithione and divalent zinc.

compounds that promote self-interaction of TIA-1. In the course of performing an initial compound screen, we identified pyrithione zinc as a potent upregulator of TIA-1 multimerization *in vitro*. We then determined that the Zn^{2+} moiety of pyrithione zinc was responsible for the enhanced FRET signal and that Zn^{2+} was sufficient to induce phase separation of recombinant TIA-1, which in turn could be reversed by the zinc chelator, TPEN. In cultured cells, TPEN also inhibited the formation of TIA-1-positive stress granules normally induced by arsenite treatment while promoting the expulsion of TIA-1 from pre-formed stress granules. Although zinc alone was insufficient to induce stress granule assembly in cells, it potentiated the effects of arsenite. Finally, in cultured cells loaded with the zinc-specific fluorescent probe FluoZin-3 AM, release of Zn^{2+} was detected within minutes of treatment with sodium arsenite, well before the appearance of stress granules. These results indicate that the formation of TIA-1-positive stress granules is dynamically regulated by zinc, which is released during cellular stress and induces reversible multimerization and phase separation of TIA-1.

RESULTS

Zn^{2+} Induces Reversible Self-Multimerization of Recombinant TIA-1

We devised a FRET-based assay to identify small molecules that promote homomeric TIA-1 interaction *in vitro*, with the goal of developing molecular tools to investigate the biological function of TIA-1 aggregation. Briefly, recombinant TIA-1-ECFP and TIA-1-EYFP were incubated together at a final concentration of approximately 130 nM each (10 μg/mL), followed by addition of various test compounds from a compound library. Donor FRET was then measured using a microplate reader. In this assay, FRET occurs when the ECFP and EYFP tags are brought close to each other because of interaction between the TIA-1 proteins to which they are tethered (Figure 1A). Thus, a compound that promotes multimerization of TIA-1 would reduce apparent fluorescence of the donor fluorescent protein (TIA-1-ECFP), because a portion of the emitted energy would be absorbed by the acceptor (TIA-1-EYFP) (Figure 1A).

A compelling hit to emerge from this screen was pyrithione zinc, a compound that exists in equilibrium with free pyrithione and divalent zinc under aqueous conditions (Figure 1B). Pyrithione zinc (PZ) exhibited a dose response in the FRET assay over a concentration range of 0–12.5 μM, with donor FRET peaking (i.e., reaching minimal ECFP fluorescence versus baseline reading at 0 min) within approximately 10–15 min of incubation at the upper range of PZ concentration (Figure 2A). Zinc chloride yielded precisely the same effect as PZ (Figure 2B). Concentrations of 25, 50, and 100 μM of either zinc compound produced erratic FRET measurements because of a tendency to precipitate the recombinant proteins and were therefore excluded from the two-fold dilution series used in the FRET assay (data not shown). Fitting the latter dose-response data to a sigmoidal function, PZ and $ZnCl_2$ yielded half-maximal effective concentration (EC_{50})s of 0.78 and 0.77 μM, respectively (Figure 2C).

To ensure interpretability of the FRET assay and to establish specificity for Zn^{2+}, we performed several control experiments. First, we found that neither free pyrithione (Figure 2D) nor the divalent cations, Ca^{2+} and Mn^{2+} (Figures 2E and S1A), produced a dose response, although we could not evaluate the effects of Cu^{2+} because of its fluorescence-quenching properties (data not shown) (Dean et al., 2012). To rule out that Zn^{2+}-dependent FRET was caused by TIA-1-independent interaction of ECFP and EYFP, the assay was performed with recombinant His-ECFP substituted for His-TIA-1-ECFP. In this case, Zn^{2+} did not produce a dose response (Figure 2F), which is important to

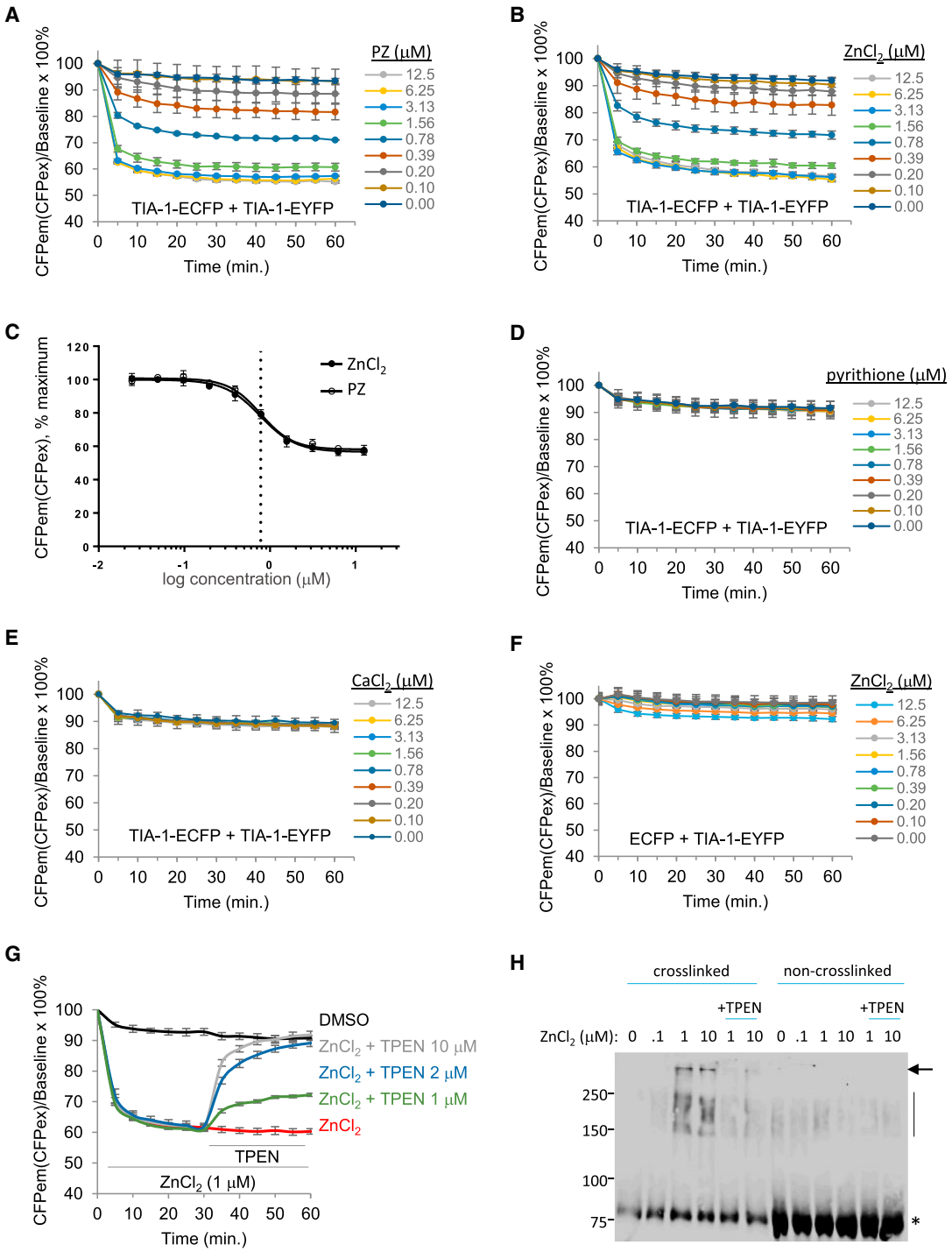

Figure 2. Self-Multimerization of TIA-1 Is Specifically Regulated by Zn^{2+} *In Vitro*

(A and B) Dose dependency of donor FRET on (A) PZ and (B) zinc chloride. $p < 0.0001$ for the main effect of concentration for both compounds, rmANOVA.
(C) EC_{50} calculation for PZ (0.78 μM, $R^2 = 0.997$) and $ZnCl_2$ (0.77 μM, $R^2 = 0.997$), indicated by the vertical dotted line.
(D–F) Absence of dose response for (D) pyrithione or (E) Ca^{2+} or (F) if His-ECFP is substituted for TIA-1-ECFP.
(G) Dose-dependent reversibility of Zn^{2+}-dependent FRET by TPEN *in vitro*. $p < 0.0001$ for the main effect of TPEN concentration, rmANOVA. FRET data are from triplicate samples and expressed as means ± SEM, except for the EC_{50} graph, which expresses means ± SD.
(H) *In vitro* crosslinking of recombinant TIA-1-ECFP followed by SDS-PAGE and immunoblot showing multimeric TIA-1 species (>150 kDa) as a function of zinc concentration, reversible by subsequent incubation with TPEN (10 μM). Monomeric, di- or trimeric, and unresolvable higher-weight TIA-1 species are indicated by an asterisk, line, and arrow, respectively. Experiments were repeated at least 3 times, with representative data shown.

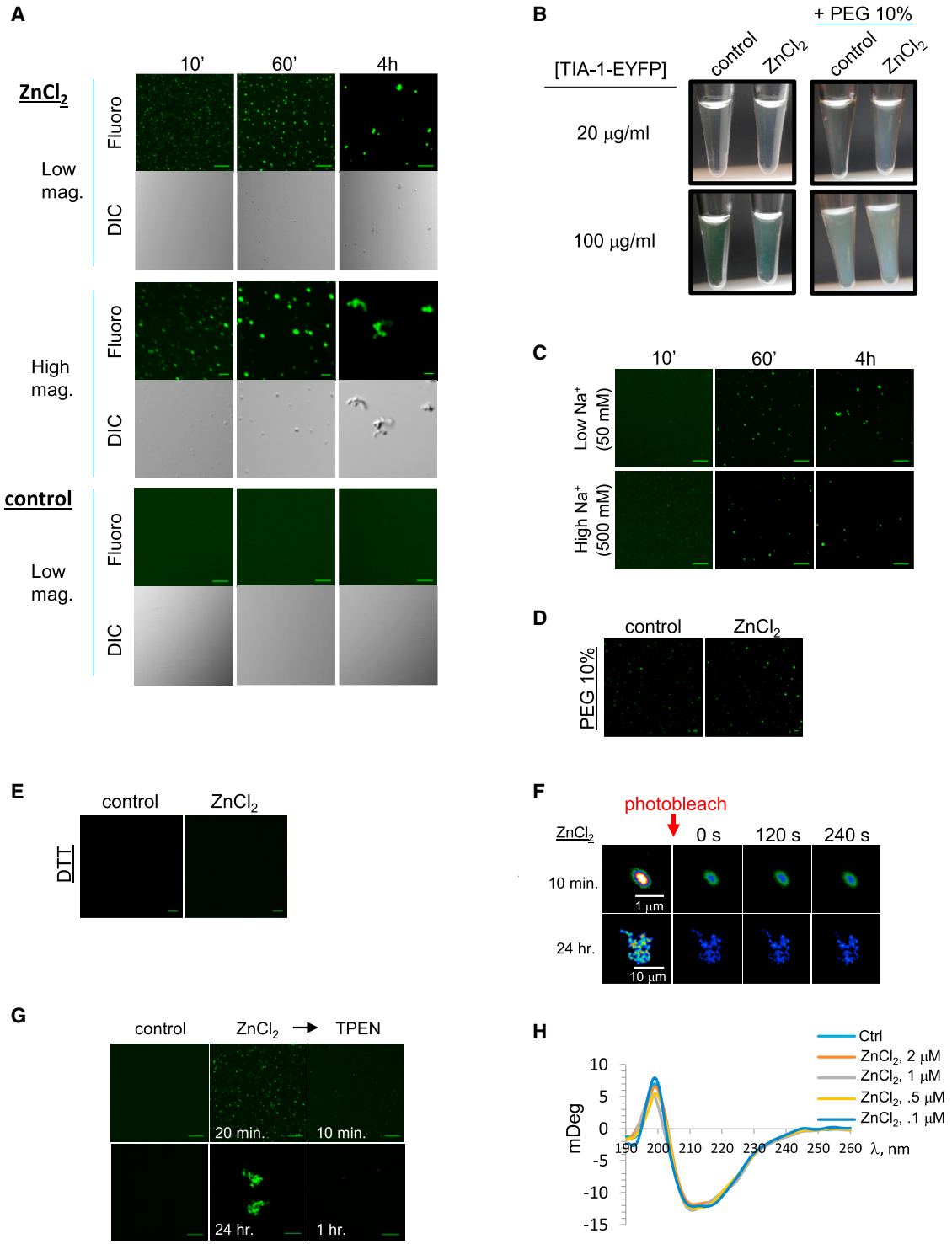

Figure 3. Zinc-Induced Phase Separation of Recombinant TIA-1 Is Reversible and Not Associated with Changes in β Sheet Content

(A) Confocal and DIC imaging of phase separation of recombinant TIA-1-EYFP as a function of time ± 1 μM $ZnCl_2$. For low- and high-magnification images, scale bars represent 10 and 2 μm, respectively.

(B) Turbidity of TIA-1-EYFP mixtures as a function of protein concentration, $ZnCl_2$ (1 μM), and PEG.

(C) Phase separation of TIA-1-EYFP as a function of time and salt concentration. Scale bars represent 10 μm.

(D and E) Phase separation of as a function of (D) PEG 10% and (E) 1 mM DTT. Scale bars represent 2 μm.

(legend continued on next page)

establish because Zn^{2+} can promote dimerization of His-tagged proteins under certain experimental conditions (Evers et al., 2008). In addition, there was no impact of Zn^{2+} on inherent fluorescence of TIA-1-EYFP (Figure S1B), or on TIA-1-ECFP fluorescence in isolation (Figure S1C). In addition, we observed comparable effects of Zn^{2+} in the FRET assay under four buffer conditions—sodium phosphate buffer (the primary buffer used in this study), PIPES, HEPES, and Tris (Figure S1D)—ruling out potentially confounding effects of buffer-metal interaction.

To determine whether Zn^{2+}-dependent multimerization of TIA-1 in the FRET assay was reversible, recombinant TIA-1-ECFP and TIA-1-EYFP were incubated in the presence of 1 μM $ZnCl_2$ (a concentration that slightly exceeds the EC_{50} calculated earlier) before addition of TPEN. Fluorescence of TIA-1-ECFP treated with Zn^{2+} approached minimal levels by approximately 10–15 min, but the FRET signal was rapidly reversed in a dose-dependent manner following addition of the zinc chelator TPEN (Figure 2G).

With the goal of visualizing the multimeric configurations of TIA-1 that may contribute to a positive FRET signal in the latter assays, we next performed an *in vitro* crosslinking assay with recombinant TIA-1, followed by SDS-PAGE and immunoblot. At Zn^{2+} concentrations shown to elicit donor FRET (1 and 10 μM), we observed a strong increase in the intensity of diffuse bands in the 150–250 kDa range, which conceivably reflects dimeric and trimeric species of heterogeneous conformation (Figure 2H). Multimeric complexes beyond the trimer range were also visible with the latter concentrations of $ZnCl_2$, but these barely entered the resolving layer of the gel, if at all. However, no such signals were comparably observed in the 0 or 0.1 μM $ZnCl_2$ lanes or if samples were not crosslinked. Significantly, addition of TPEN after zinc treatment caused a collapse of the high molecular species present in the crosslinked 1 μM and 10 μM $ZnCl_2$ samples. These data suggest that the FRET signal observed in the previous assays is caused by TIA-1 multimers that are 150 kDa or larger that interact in a reversible and non-covalent manner in the presence of Zn^{2+}. Although equivalent amounts of material were loaded into each well, the immunoreactivity of crosslinked samples was reduced in comparison to non-crosslinked samples, which is ostensibly a consequence of altered epitope accessibility caused by formaldehyde treatment. Altogether, the FRET and SDS-PAGE experiments indicate that Zn^{2+} directly binds recombinant TIA-1 *in vitro*, triggering reversible self-multimerization of the protein.

Zn^{2+} Promotes Reversible Phase Separation of Recombinant TIA-1 without Altering β Sheet Content

Aggregation-prone proteins such as TIA-1 are characterized by the presence of IDRs that promote phase separation, a phenomenon by which a protein solute undergoes demixing to form a suspension of liquid-like droplets (Kato et al., 2012; Lin et al., 2015). Phase separation has been suggested to underlie the formation of stress granules, processing bodies (P-bodies), nucleoli, and other membrane-less subcellular compartments (Shin and Brangwynne, 2017). In light of these observations, and because of the limited ability of SDS-PAGE to resolve large multimeric complexes, we explored the possibility that recombinant TIA-1 protein might undergo phase separation in a zinc-dependent manner.

In vitro reactions were assembled under conditions employed during the FRET assay, but samples were instead examined by confocal and differential interference contrast (DIC) microscopy. Within 10 min of adding 1 μM $ZnCl_2$ to TIA-1-EYFP, droplets 0.1–1 μm in diameter were observed in both the fluorescence and the DIC channels, but not in untreated samples (Figure 3A). Within the first hour of incubation, the zinc-induced droplets maintained a spherical appearance, growing in size while becoming sparser. However, by 4 hr, the morphology assumed a larger, irregular, and more fibrillar appearance. In parallel to the microscopy data, we found that solutions of TIA-1-EYFP developed visible turbidity that varied positively with protein concentration, zinc addition, and molecular crowding by polyethylene glycol (PEG) addition (Figure 3B). Similar results were obtained for TIA-1-ECFP (data not shown). Under the conditions of the FRET assay (20 μg/mL of protein and no PEG), no turbidity was observed in the absence of zinc (Figure 3B), and there was negligible droplet formation in imaged samples at a sub-EC_{50} dose of $ZnCl_2$ (0.1 μM) (Figure S2). These results demonstrate a high degree of consistency among the different *in vitro* assays used in this study.

Key factors that influence phase separation of aggregation-prone proteins are salt concentration and molecular crowding (Lin et al., 2015; Nott et al., 2015). In comparison to the standard buffer conditions used in the previous experiments (150 mM NaCl), both low and high salt (50 and 500 mM NaCl, respectively) caused a reduction in droplet size, droplet number, and rate of droplet formation (Figures 3A and 3C), emphasizing the importance of optimal electrostatic interactions to drive the formation of higher-order TIA-1 condensates. Incubating TIA-1-EYFP with 10% PEG induced the formation of TIA-1 droplets in the absence of Zn^{2+} (Figure 3D). However, droplet size and number were further increased in the presence of Zn^{2+}, while zinc-dependent FRET still exhibited a dose response in the presence of 10% PEG (Figures 3D and S3A), suggesting that zinc treatment and molecular crowding have a cumulative effect on phase separation of TIA-1. Finally, addition of DTT to simulate the reducing environment of the cell prevented the formation of TIA-1 droplets normally induced by 1 μM $ZnCl_2$ and eliminated the zinc dose response in the FRET assay (Figures 3E and S3B), consistent with the idea that TIA-1 multimerization is responsive to both zinc and reduction-oxidation (redox) environment.

To determine whether the droplets observed in the latter assays were in a state of dynamic flux, TIA-1-EYFP droplets were

(F) FRAP analysis of TIA-1-EYFP aggregates induced by 1 or 24 hr $ZnCl_2$ (1 μM) incubation *in vitro*.
(G) Phase separation of TIA-1-EYFP induced by 1 μM ZnCl2 for 20 min, followed by an additional 10 min with TPEN (20 μM) or 24 hr followed by addition of TPEN for 1 hr. Scale bars represent 10 μm. Representative images from at least three independent experiments are shown.
(H) CD analysis of TIA-1 as a function of zinc concentration. BestSel algorithm (Micsonai et al., 2015) estimations of α helix and β sheet content are approximately 18% and 25%, respectively, for all conditions shown (normalized root mean square deviation [NRMSD] < 0.05).

again formed *in vitro* by incubation with 1 μM $ZnCl_2$ for either 10 min or 24 hr, followed by photobleaching and subsequent monitoring of fluorescence recovery. We found no recovery of fluorescence over the course of 4 min post-photobleaching, suggesting a relatively static structural configuration of both types of condensates (Figure 3F). The TIA-1-EYFP condensates induced by brief incubation with Zn^{2+} were all but eliminated by TPEN (Figure 3G), consistent with earlier observations from both FRET and SDS-PAGE data. We found that the large irregular structures formed after 24 hr incubation of TIA-1-EYFP with zinc were also reversible (Figure 3G).

Conversion of prions from a soluble to an aggregation-prone conformation is often accompanied by an increase in β sheet content (Pan et al., 1993). However, this is not necessarily the case for all prion-related proteins, such as the immunological protein MAVS (Hou et al., 2011). To determine whether zinc-dependent multimerization of recombinant TIA-1 is associated with changes in β sheet content, we analyzed recombinant TIA-1 by circular dichroism (CD) spectroscopy. Virtually identical CD spectra were obtained for a range of $ZnCl_2$ concentrations encompassing the EC_{50} determined earlier (Figure 3H). Estimates of secondary structure content were approximately 26% α helix and 31% β sheet for all conditions. We conclude that the zinc-dependent changes in TIA-1 multimerization are not accompanied by major secondary structure alterations.

Intracellular Zinc Is Released in Response to Arsenite Treatment

To determine whether interaction between TIA-1 and Zn^{2+} *in vitro* is likely to be physiologically relevant, it is important to establish whether zinc is released during cellular stress. To investigate this possibility, we loaded HT22 cells with the membrane-permeable zinc-specific fluorescent probe, FluoZin-3 AM, followed by treatment with sodium arsenite (NaAs), a potent inducer of both stress granule formation and oxidative stress. Treatment with NaAs for 10 min elicited almost a three-fold increase in FluoZin-3 AM fluorescence versus untreated control cells, while 1 μM PZ increased fluorescence by more than eight-fold (Figures 4A and 4B). FluoZin-3 AM fluorescence exhibited prominent cytoplasmic localization for all three treatment groups. The punctate and perinuclear fluorescence is characteristic of lysosomal and possibly Golgi association of this particular zinc probe (McCormick et al., 2010; Muylle et al., 2006). NaAs had no direct effect on FluoZin-3 fluorescence in isolation (Figure S4).

To corroborate these data, a similar experiment was performed in mouse hippocampal slices loaded with FluoZin-3 AM and treated with NaAs. For this purpose, we adapted a temperature- and CO_2-controlled microplate reader to sample fluorescence emission in a slice preparation. For vehicle-treated slices, FluoZin-3 AM fluorescence remained stable during the duration of the experiment (Figure 4C). However, slices treated with NaAs exhibited a significant increase in fluorescence after 5 min of incubation, which continued to increase until peaking at 25 min (Figure 4C). These results are in good agreement with the imaging data from HT22 cells (Figures 4A and 4B) and demonstrate that arsenite-induced zinc release is not a phenomenon restricted to cell lines.

Zinc Chelation Blocks the Formation and Maintenance of TIA-1-Positive Stress Granules in HT22 Cells

We next asked whether release of Zn^{2+} during cellular stress had any impact on endogenous TIA-1 and its role in stress granule formation. First, we pre-treated HT22 cells with TPEN, which is membrane permeable, and then we exposed the cells to NaAs. Stress granules were typically detected 20–30 min after incubation with arsenite (Figure S5), occurring well after the rise in intracellular zinc (Figure 4). Both vehicle- and TPEN-treated cells exhibited diffuse TIA-1 immunofluorescence throughout the soma and nucleus (Figures 5A and 5B). Another classical stress granule marker, G3BP, showed diffuse localization throughout the cytoplasm in both vehicle- and TPEN-treated cells (Figures 5A and 5C). Arsenite treatment produced a robust increase in stress granule frequency, indicated by the presence of cytoplasmic foci $\geq$ 0.5 μm in diameter staining positive for TIA-1 or G3BP (Figure 5). Co-localization of these classical stress granule markers was qualitatively very high, as expected (Figure 5A, merged images). However, in cells pre-treated with TPEN followed by NaAs, the number of TIA-1-positive stress granules was significantly reduced (Figure 5B), while there was no significant impact on the number of G3BP-positive foci (Figures 5A and 5C). The TIA-1-related protein TIAR behaved similarly to G3BP in these experiments, forming arsenite-induced cytoplasmic foci that were relatively insensitive to zinc chelation (Figure S6). Thus, the effects of zinc chelation on stress granule assembly in HT22 cells appear to be specific to TIA-1, with little or possibly no role in the recruitment of at least two other stress granule markers, G3BP and TIAR.

Given that Zn^{2+} is important for the recruitment of TIA-1 into stress granules at the onset of cellular stress, we investigated whether Zn^{2+} was also necessary for retention. Thus, HT22 cells were treated with NaAs for 30 min, followed by addition of TPEN. We found a significant reduction in TIA-1-positive stress granules in cells treated with both arsenite and TPEN versus arsenite alone (Figures 6A and 6B). In contrast, there was no difference in the number of G3BP-positive foci (Figures 6A and 6C). These results indicate that zinc chelation also interferes with retention of TIA-1 in stress granules.

Divalent Zinc Stimulates the Effect of Arsenite on Stress Granule Assembly

To determine whether Zn^{2+} alone is sufficient to induce the formation of stress granules, PZ was bath-applied to HT22 cells, followed by confocal microscopy to quantitate the number of stress granules per cell. While arsenite treatment reliably produced TIA-1-, TIAR-, and G3BP-positive stress granules in HT22 cells, PZ alone did not (Figure 7), although 1 μM PZ was sufficient to produce enhancement of FluoZin-3 AM fluorescence significantly exceeding that generated by 0.5 mM NaAs (Figures 4A and 4B). However, PZ potentiated the effects of low NaAs concentration (100 μM) on TIA-1-positive stress granule formation (Figure 7) while enhancing recruitment of G3BP. In summary, while zinc is insufficient to promote stress granule assembly on its own, it can potentiate the effect of arsenite.

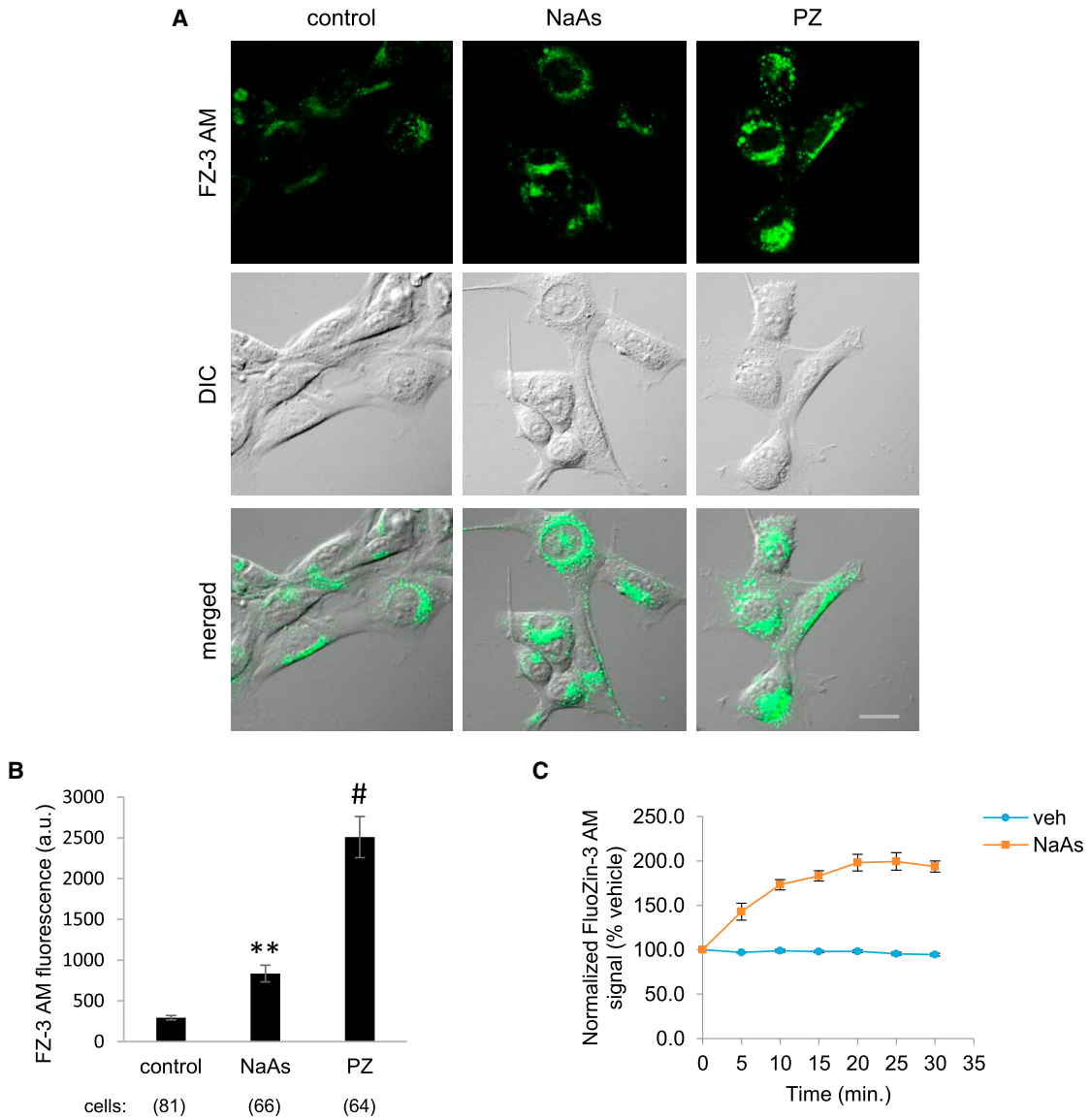

Figure 4. Intracellular Zinc Release in HT22 Cells Is Triggered by NaAs

(A) Confocal images of HT22 cells loaded with FluoZin-3 AM revealing significant enhancement of zinc-dependent fluorescence after treatment with 0.5 mM NaAs or 1 μM PZ. Representative fields from 3 independent experiments are shown. Scale bar represents 20 μm. Brightness of the fluorescence signal was enhanced in the merged images to improve visibility.

(B) Quantitation of FluoZin-3 AM fluorescence (control, 293.0 ± 0.59 a.u.; arsenite, 834.9 ± 0.41 a.u.; PZ, 2,508.9 ± 1.84 a.u.). **$p < 0.01$ and #$p < 0.0001$ versus control, one-way ANOVA, Fisher's post hoc test.

(C) Rapid enhancement of zinc release in mouse hippocampal slices loaded with FluoZin-3 AM. $p < 0.0001$ for the main effect of arsenite treatment, rmANOVA ($n = 5$ slices per condition). Data are means ± SEM.

DISCUSSION

In contrast to pathological prions such as PrP^{Sc}, which are associated with neurodegenerative disease, TIA-1 belongs to a nascent class of functional prion-like proteins that includes the translational regulators CPEB3 in mouse, ApCPEB in *Aplysia*, and Orb2 in *Drosophila* and the immune response protein MAVS (Fioriti et al., 2015; Hou et al., 2011; Li et al., 2014; Majumdar et al., 2012; Rayman and Kandel, 2017a, 2017b; Si et al., 2003; Stephan et al., 2015). Functional prion-like proteins are distinguished from their pathogenic counterparts in that their aggregation both is regulated and serves a positive physiological function. However, the structure-function relationship of prions and prion-like proteins remains difficult to elucidate, in part because of the scarcity of high-resolution structures of aggregated conformations (Diaz-Espinoza and Soto, 2012). In addition, the genetic and biochemical approaches used to study aggregation-prone proteins generally do not target

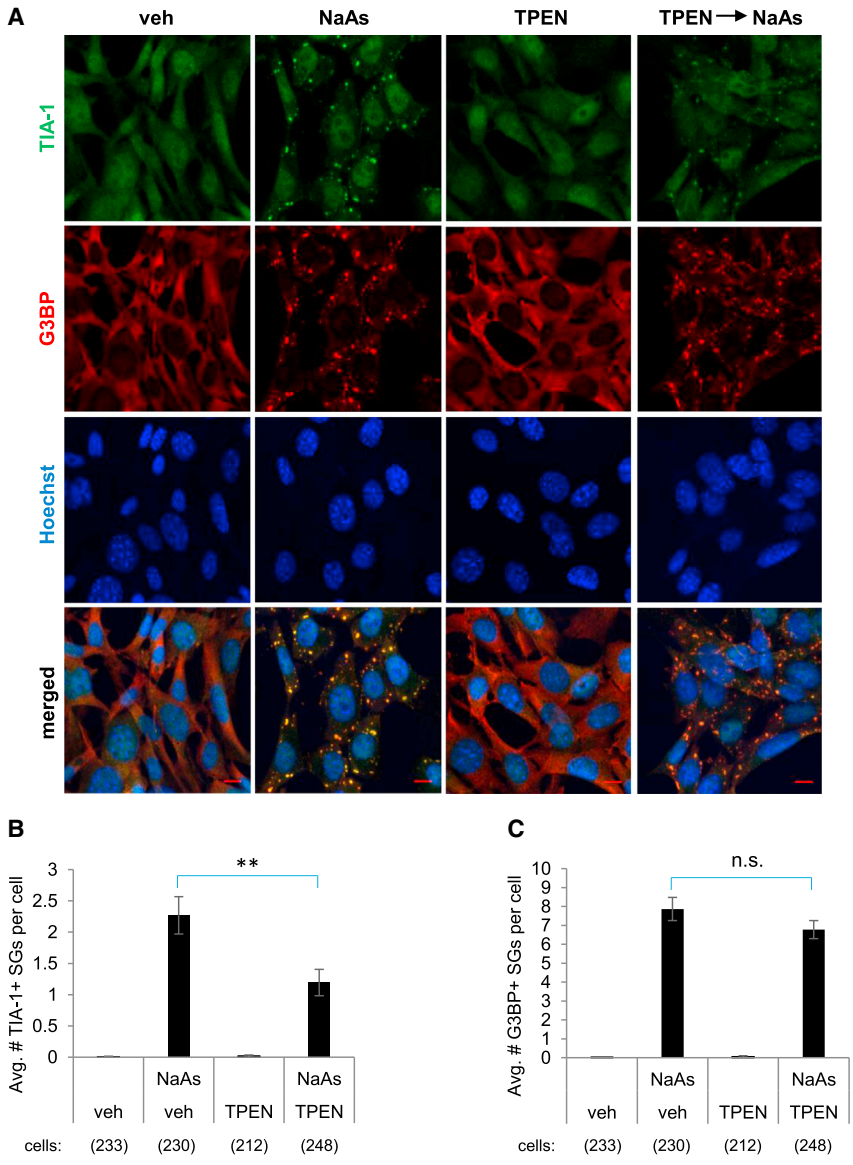

Figure 5. Localization of TIA-1 into Stress Granules during Arsenite Treatment Is Regulated by Divalent Zinc

(A) Confocal images of HT22 cells treated with vehicle, TPEN (20 μM), NaAs (0.5 mM), or TPEN + NaAs, and stained with anti-TIA-1 (green channel) and anti-G3BP (red channel) antibodies. Cells were preincubated with either vehicle [veh] or TPEN for 40 min, followed by arsenite for an additional 30 min. Scale bars represent 10 μm.

(B) Quantitation of images demonstrating that TPEN pre-incubation inhibits arsenite-induced stress granule (SG) formation (veh, 0.0 ± 0.01 SGs per cell; NaAs, 2.3 ± 0.30 SGs per cell; TPEN, 0.0 ± 0.02 SGs per cell; NaAs+TPEN, 1.2 ± 0.21 SGs per cell). **$p < 0.01$ for the arsenite-TPEN interaction, two-way ANOVA.

(C) Quantitation of G3BP-positive stress granules showing robust induction by NaAs treatment but no effect of TPEN (veh, 0.0 ± 0.01 SGs per cell; NaAs, 7.9 ± 0.62 SGs per cell; TPEN, 0.1 ± 0.05 SGs per cell; NaAs+TPEN, 6.8 ± 0.48 SGs per cell). $p > 0.05$ for the arsenite-TPEN interaction, two-way ANOVA. Data represent averages from 3 independent experiments. Error bars represent means ± SEM.

aggregation per se, often relying on overexpression-based strategies or deletion of key domains that probably affect more than self-multimerization.

With these issues in mind, we embarked on the development of molecular tools with which to probe the structure and physiological function of aggregated TIA-1. Following up on positive findings from an *in vitro* screen of a compound library, our search for an artificial ligand of TIA-1 led to the discovery of a natural ligand—divalent zinc. Along with the initial FRET-based screen, we conducted two sets of *in vitro* assays (SDS-PAGE and phase separation) that independently demonstrated robust and reversible multimerization of recombinant TIA-1 induced by Zn^{2+}. These results support the idea that IDR-containing proteins can adopt a range of structural configurations depending on environmental conditions, thus conferring specific biochemical and biophysical properties to the non-membrane-limited condensates that they may form in cells (Shin and Brangwynne, 2017). It is tempting to speculate that zinc-dependent condensation of TIA-1 offers a reversible and specific means of providing structural stability to droplet cores, which are more stable than the shell region with which cellular materials are readily exchanged, although earlier studies suggest that interaction of TIA-1 with stress granules is dynamic (Bley et al., 2015; Jain et al., 2016; Kedersha et al., 2005). However, differences in cell type, construct type, and stressor, as well as the effects of overexpressing an IDR-containing protein per se, have not been systematically addressed in the literature, and distinct outcomes might be observed under different experimental conditions.

Building on the latter *in vitro* results, we determined in cell culture experiments that chelation of Zn^{2+} by TPEN before arsenite treatment inhibited the recruitment of TIA-1 into stress granules. Conversely, stress granule induction followed by TPEN treatment caused a decrease in the number of TIA-1-positive stress granules. In addition, while exogenous Zn^{2+} on its own was insufficient to promote the formation of TIA-1-positive stress granules, it potentiated the effects of arsenite on recruitment of TIA-1. DTT prevented both zinc-dependent phase separation and homomeric interaction of TIA-1 (FRET assay), which suggests that both zinc release and redox changes are necessary to trigger multimerization (Figures 3E and S3B). Furthermore, in contrast to the zinc chelation experiments showing no evidence of zinc-dependent recruitment of G3BP, we observed that

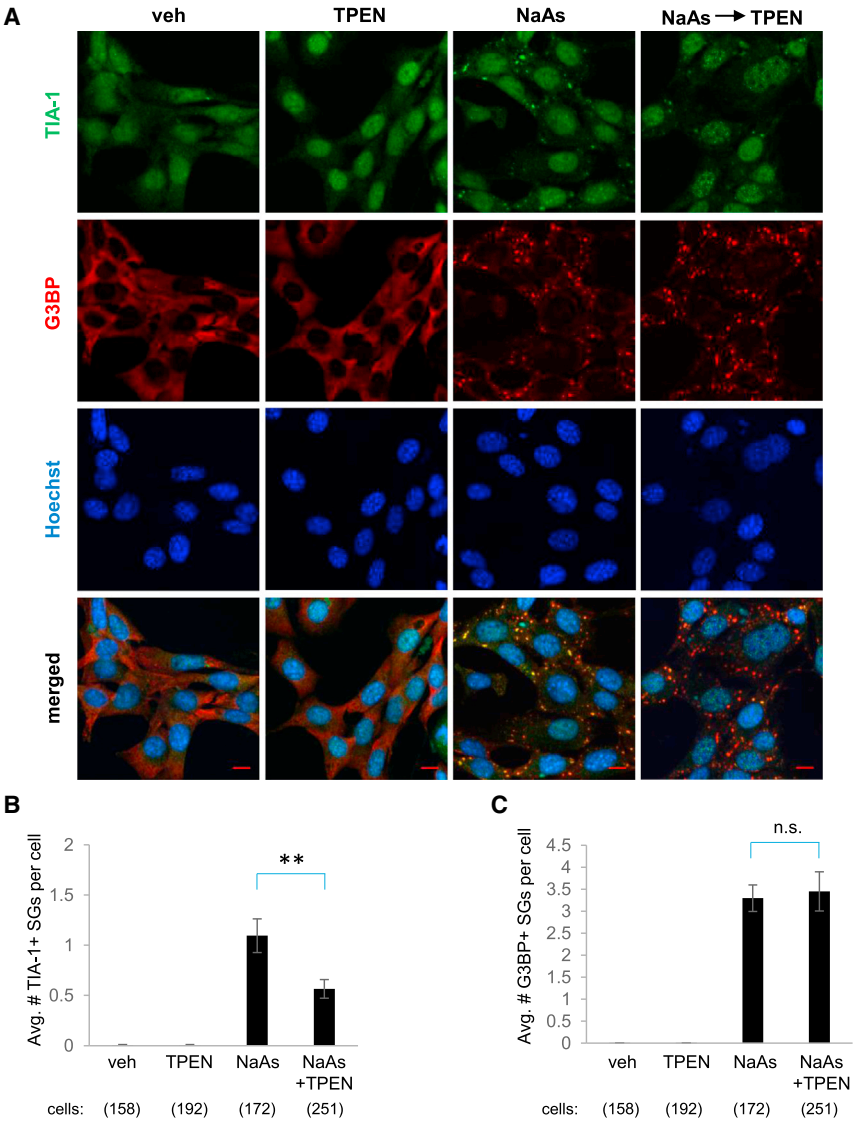

Figure 6. TPEN Causes a Reduction in the Number of Pre-Formed TIA-1-Positive Stress Granules

(A) Confocal images of HT22 cells exposed to arsenite (0.5 mM) for 30 min, followed by TPEN (20 μM) for an additional 30 min, and then stained for TIA-1 and G3BP. Representative images from 3 independent experiments. Scale bars represent 10 μm.

(B) Quantitation of TIA-1+ foci showing TPEN-dependent reduction of pre-formed TIA-1+ SGs (veh, 0.0 ± 0.01 SGs per cell; TPEN, 0.0 ± 0.00 SGs per cell; NaAs, 1.1 ± 0.17 SGs per cell; NaAs+TPEN, 0.6 ± 0.09 SGs per cell). **$p < 0.01$ for the arsenite-TPEN interaction, two-way ANOVA.

(C) Quantitation of G3BP+ foci showing no effect of TPEN (veh, 0.0 ± 0.00 SGs per cell; TPEN, 0.0 ± 0.00 SGs per cell; NaAs, 3.3 ± 0.30 SGs per cell; NaAs+TPEN, 3.4 ± 0.45 SGs per cell). $p > 0.05$ for the arsenite-TPEN interaction, two-way ANOVA. Data represent averages from 3 independent experiments. Error bars represent means ± SEM.

exogenous Zn^{2+} increased the number of G3BP-positive stress granules, which may be a reflection of secondary effects of zinc exposure that are not entirely reciprocal to zinc chelation.

Stress granules are compositionally heterogeneous structures that do not strictly require TIA-1 (Bley et al., 2015; Bounedjah et al., 2014). Both TIA-1 and G3BP foci are robustly induced by arsenite treatment, and essentially all TIA-1 foci co-localized with G3BP. However, many G3BP foci did not co-localize with TIA-1 (Figures 5, 6, and 7), demonstrating that a subpopulation of stress granules is G3BP positive but TIA-1 negative, although differences in antibody performance and epitope accessibility may be factors. Given that zinc chelation had little effect on other stress granule markers such as G3BP and TIAR (Figures 5C and S6), our results support a specific role for the interaction of TIA-1 with Zn^{2+} during the assembly of stress granules. Further studies are needed to characterize the functional differences between these granule subtypes.

There has been scant mechanistic detail regarding the functional links among signaling events, concomitant changes in TIA-1 structure and function, and stress granule formation. In one example, TIA-1 was found to be regulated by reactive oxygen species, which covalently modify a key cysteine residue in the protein, leading to suppression of stress granule formation (Arimoto-Matsuzaki et al., 2016). However, our study has identified a molecular signaling event that directly promotes both self-multimerization and recruitment of TIA-1 into stress granules. Our data, along with the results of other studies, can be incorporated into a model for zinc-dependent regulation of TIA-1 that has the following features. Exposure to arsenite (or other redox stressor) produces an increase in free zinc, which may be released from redox-sensitive metallothioneins (Hall et al., 1999; Oteiza, 2012). Zinc subsequently binds to cytoplasmic TIA-1, causing homomeric aggregation and phase separation that are not strictly dependent on changes in β sheet content or the presence of RNA. Together with the accumulation of untranslated messenger ribonucleoprotein (mRNP) complexes arising from stress-dependent phosphorylation of eIF2α, the multimerization of TIA-1 and other IDR-containing proteins establishes a kinetically favorable network of noncovalent protein-protein and protein-RNA interactions that becomes manifest as stress granules (Anderson and Kedersha, 2002; Dyson and Wright, 2005; Shin and Brangwynne, 2017). Other post-translational events that contribute to stress granule assembly include phosphorylation, neddylation, and *O*-Glc-Nac glycosylation of stress granule components (Jayabalan et al., 2016; Ohn et al., 2008; Tourrière et al., 2003). The coordinated

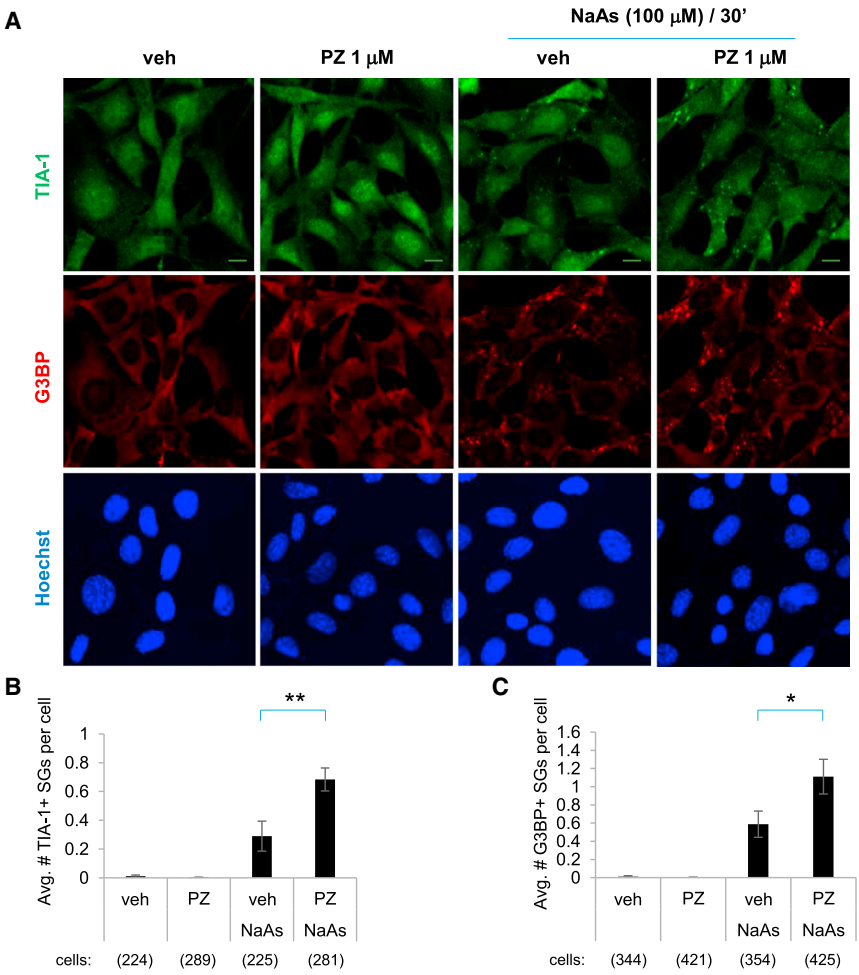

Figure 7. Treatment of HT22 Cells with PZ Potentiates the Effect of a Low Dose of Arsenite on Stress Granule Formation

(A) Confocal images of TIA-1 (green) and G3BP (red) staining of HT22 cells treated with PZ (1 μM) and/or low NaAs concentration (100 μM). Scale bar represents 10 μm.

(B) Quantitation of TIA-1 foci from 3 independent experiments shows potentiation of arsenite-induced TIA-1-positive stress granules by PZ (veh, 0.0 ± 0.01 SGs per cell; PZ, 0.0 ± 0.00; veh/NaAs, 0.3 ± 0.10 SGs per cell; PZ/NaAs, 0.7 ± 0.08 SGs per cell). **$p < 0.01$ for the arsenite-PZ interaction, two-way ANOVA.

(C) Quantitation of G3BP foci from 5 independent experiments showing potentiation of arsenite-induced stress granules by PZ (veh, 0.0 ± 0.01 SGs per cell; PZ, 0.0 ± 0.00 SGs per cell; NaAs, 0.6 ± 0.14 SGs per cell; PZ/NaAs, 1.1 ± 0.19 SGs per cell). *$p < 0.05$ for the arsenite-PZ interaction, two-way ANOVA. Data are means ± SEM.

actions of these post-translational events presumably allow a finely tunable, dynamic cellular response to prevailing environmental conditions.

Zinc plays important roles in a diverse range of biological processes, including cellular signaling, immune function, and synaptic plasticity, and is a co-factor for many structural proteins, transcription factors, and enzymes (Hojyo and Fukada, 2016; Liang et al., 2016; Oteiza, 2012; Takeda et al., 2014; Yamasaki et al., 2007). Particularly relevant to this study is Zn^{2+} being intimately connected with a variety of redox signaling pathways (Oteiza, 2012) and therefore poised to act as a barometer of cellular redox state. Major perturbations of redox state can have detrimental consequences on cell survival and must be rapidly interpreted by signaling systems to execute an adaptive cellular response and maintain homeostasis. Divalent zinc is highly suited as a second messenger in this regard, given its involvement in redox signaling and its ability to regulate stress granule dynamics by modulating TIA-1 multimerization. The diverse roles of zinc in cellular physiology highlight an important limitation of this study, which is that our data cannot distinguish between direct and indirect effects of Zn^{2+} on stress granule formation. For example, stress-dependent release of intracellular zinc may activate zinc-responsive kinases or structural proteins that are critical for stress granule assembly. These pathways could additionally regulate TIA-1 multimerization and stress granule formation, independent of the effects of direct interaction between Zn^{2+} and TIA-1.

In retrospect, it is not surprising that Zn^{2+} regulates the aggregation of prion-related proteins such as TIA-1. Many examples of interactions between zinc and prion- and amyloid-like proteins have been described, although chiefly in a pathophysiological context. For example, the kinetics and structure of human prion protein during aggregation are sensitive to Zn^{2+} (Pan et al., 2015), as is the misfolding of β-amyloid (Matheou et al., 2016). However, TIA-1 is a prion-related protein whose physiological aggregation is dynamically regulated by zinc. It will be important to determine the extent to which the structural and kinetic properties of aggregated TIA-1 are comparable to those of other prion-related proteins with respect to zinc modulation.

In conclusion, we have found that Zn^{2+} is rapidly released during arsenite treatment and is necessary for efficient recruitment of TIA-1 into stress granules, as well as retention. Both *in vitro* data and cell culture studies are consistent with the idea that Zn^{2+} promotes homomeric multimerization and phase separation of TIA-1, which in turn drives the assembly of TIA-1-positive stress granules. These discoveries may reveal general principles that govern both physiological and pathological aggregation of prion-like proteins.

EXPERIMENTAL PROCEDURES

Cloning, Expression, and Purification of Recombinant TIA-1

His-tagged TIA-1-ECFP and TIA-1-EYFP were generated by standard recombinant DNA methods. The open reading frame (ORF) encoding the 386 amino acid isoform of TIA-1 was cloned from a mouse C57BL/6 cDNA library into the

pRSET expression vector (Thermo Fisher Scientific) upstream of either ECFP or EYFP to generate His-tagged fusion proteins. The plasmids were verified by sequencing and used to transform BL21AI cells (Thermo Fisher Scientific) for arabinose-inducible expression, followed by standard purification using a nickel resin. Purified proteins were dialyzed against 2× PBS and 50% glycerol and adjusted to equal concentration by SDS-PAGE or Coomassie stain and optical density 280 nm (OD_{280}).

FRET-Based Compound Screen and Analysis

100 μL reactions were assembled in non-binding 96-well glass-bottom plates (Costar), with 1 μg (~130 nM final concentration) of TIA-1-ECFP, TIA-1-EYFP, or both in phosphate buffer (10 mM NaH_2PO_4, 150 mM NaCl). Compounds from a U.S. Food and Drug Administration (FDA)-approved library (Selleckchem) were added at indicated concentrations using DMSO as vehicle. Samples were run in triplicate and top-read every 5 min for 1 hr at 25°C in a CLARIOStar microplate reader (BMG) using three excitation and monochromator combinations to measure CFPem (CFPex), YFPem (CFPex), and YFPem (YFPex): (1) CFPex 430 ± 15 nm, dichroic 457.5 nm, CFPem 480 ± 10 nm; (2) CFPex 430 ± 15 nm, dichroic 505 nm, YFPem 530 ± 10 nm; and (3) YFPex 490 ± 5 nm, dichroic 510 nm, YFPem 530 ± 10 nm. Raw fluorescence values were background subtracted and normalized against initial baseline values for each condition. Donor FRET was expressed as a percentage reduction in TIA-1-ECFP fluorescence (ECFP emission with ECFP excitation) in the presence of TIA-1-EYFP versus baseline signal. To compute EC_{50}s, the log concentration versus the normalized FRET signal at 60 min was fit to a sigmoidal dose-response function using GraphPad software (Prism).

In Vitro Crosslinking

Reactions were assembled as in the FRET assay but using only TIA-1-ECFP. After 10 min of incubation with $ZnCl_2$, followed by an additional 10 min of incubation with TPEN (10 μM) or vehicle, samples were treated with formaldehyde (1% final concentration) for 5 min. Reactions were quenched with 300 mM glycine, diluted into protein sample buffer, heated at 50°C for 5 min, and then loaded onto a 6% SDS-PAGE gel. Anti-TIA-1 (Abcam ab40693) immunoblot was performed according to standard procedures. Blots were imaged with an Odyssey imaging system (LI-COR Biosciences).

Phase Separation

Reactions were assembled at room temperature as in the microplate reader assays, with differences in protein concentration and various additives (PEG, zinc chloride, and DTT) specified in the figures. Unless otherwise noted, the final concentration of TIA-1-EYFP was 260 nM (20 μg/mL). 5 μL of each reaction was spotted onto a glass coverslip and imaged using a 40× 1.3 numerical aperture (NA) oil immersion objective on an Olympus FluoView confocal microscope. To visualize turbidity, reactions were scaled up to 1 mL and photographed in glass test tubes. Fluorescence recovery after photobleaching (FRAP) was performed according to conventional procedures on TIA-1-EYFP condensates formed at indicated intervals of zinc treatment.

FluoZin-3 AM Assays

For quantitation of zinc release using confocal imaging, HT22 cells were grown in cell culture dishes with glass bottoms (MatTek). Cells were loaded with 1 μM FluoZin-3 AM (Thermo Fisher Scientific) and 0.02% Pluronic F-127 (Thermo Fisher Scientific) for 40 min, washed, and given fresh media. Compounds were added accordingly and imaged at indicated periods using an Olympus FluoView confocal microscope with GFP-compatible filters. Then, z series images were generated from approximately 20 × 0.3 μm slices. The fluorescence signal for a given cell was background corrected and quantitated using NIH ImageJ software.

Quantitation of zinc release in hippocampal slices was adapted to microplate reader format based on Schuh et al. (2011). Hippocampal tissue was obtained from adult wild-type C57BL/6 mice (Jackson Laboratory) in accordance with the institutional guidelines of Columbia University and NIH. Transverse slices (300 μm) were prepared in ice-cold dissection artificial cerebrospinal fluid (dACSF) (10 mM NaCl, 195 mM sucrose, 25 mM $NaHCO_3$, 10 mM glucose, 2.5 mM KCl, 1.25 mM NaH_2PO_4, 0.5 mM $CaCl_2$, 7 mM $MgCl_2$) bubbled with 95% O_2/5% CO_2 using a vibratome (Leica). Slices were immediately transferred to a room temperature (RT) bath of recording artificial cerebrospinal fluid (ACSF) (125 mM NaCl, 25 mM $NaHCO_3$, 25 mM glucose, 2.5 mM KCl, 1.25 mM NaH_2PO_4, 2 mM $CaCl_2$, 1 mM $MgCl_2$) and allowed to incubate for at least 45 min at RT before experimentation, with continuous bubbling of 95% O_2/5% CO_2. FluoZin-3 AM was added to the bath at a final concentration of 1 μM, along with Pluronic F-127 0.01% for 30 min. The ACSF bath was exchanged with fresh recording ACSF (3 washes × 10 min each) to remove excess dye and then quickly transferred to a black 96-well microplate (Costar). Each well contained a single slice submerged in ACSF, which was positioned at the bottom center of the well. The plate was loaded onto a microplate reader (BMG CLARIOStar) set to 30°C and 5% CO_2. After 1 hr of equilibration, baseline fluorescence was measured using top-read optics at 5 mm focal height, with a GFP-compatible filter set, in kinetic mode. When fluorescence signal was determined to be stable for at least 30 min, vehicle or arsenite was added to each well and measurements continued.

Cell Culture, Stress Granule Imaging, and Quantitation

HT22 cells were seeded on glass coverslips, cultured in DMEM with 10% fetal bovine serum (FBS), and maintained in a tissue culture chamber at 37°C and 5% CO_2. Cultures were approximately 70%–80% confluent on the day of an experiment. Cells were treated with compounds as indicated, followed by fixation with 4% paraformaldehyde (PFA) in PBS for 10 min at RT. Cells were washed several times with Tris buffer with Triton X-100 (TBx) (0.9% NaCl, 100 mM Tris-HCl [pH 7.4], and 0.5% Triton X-100) and then incubated in blocking buffer (3% BSA in TBx) for 1 hr at RT. The following antibodies were used: TIA-1 (Santa Cruz sc-1751 or Abcam ab40693), TIAR (Santa Cruz sc-1749), and G3BP (Abcam ab56574). Primary antibodies were diluted 1:2,000 into fresh blocking buffer, added to samples, and incubated overnight at 4°C. Samples were then washed several times in TBx, followed by addition of 1:1,000 dilution of Alexa 488- and 647-conjugated secondary antibodies in blocking buffer. After 2 hr, samples were washed in TBx several times, with Hoechst stain (10 μg/mL) added to the final wash. Coverslips were mounted onto slides using FluorSave reagent, and samples were imaged on an Olympus FluoView confocal microscope. Then, z series images (10 × 0.3 μm slices) were acquired with a 60× 1.4 NA oil immersion objective.

Stress granule quantitation was carried out by automated particle analysis using NIH ImageJ software. Briefly, summed *Z*-stack images were converted to 8-bit. The Hoechst channel was used to create a mask to remove the nuclear signal. Stress granules were arbitrarily defined as cytoplasmic foci > 0.5 μm^2 in diameter and circularity ≥ 0.1. After subtracting the background and removing the nuclear signal, brightness and contrast were set empirically, along with detection threshold, such that stress granules scored automatically in a training set were in agreement with the manual count. Analysis parameters were then applied systematically. The average number of stress granules per cell was calculated across 15–25 fields of cells for each experimental condition, pooled from at least 3 independent experiments.

CD

Assays were performed on a Jasco-1500 instrument at the Shared Chemistry Facility at New York University. Recombinant proteins were diluted into running buffer (10 mM NaH_2PO_4 and 150 mM NaCl [pH 8]) at 100 μg/mL. Samples were blanked against running buffer supplemented with dialysis buffer (2× PBS and 10% glycerol). Spectra from 190 to 260 nm were collected at 25°C, smoothed, background subtracted, and expressed as millidegrees using Spectra Manager software (Jasco). Traces were analyzed by the BestSel algorithm to estimate secondary structure content (Micsonai et al., 2015).

Statistical Analysis

Unless otherwise indicated, all data were reported as mean ± SEM. Statistical significance was tested using repeated-measures ANOVA (rmANOVA), two-way ANOVA, or t test as appropriate. Data were considered significant if $p < 0.05$. In marked figures, *$p < 0.05$, **$p < 0.01$, and #$p < 0.0001$. In cases in which multiple statistically significant effects are detected, only the most relevant are emphasized.

DATA AND SOFTWARE AVAILABILITY

The accession number for the data reported in this paper is Mendeley: https://doi.org/10.17632/w2rs3hxcyr.1.

SUPPLEMENTAL INFORMATION

Supplemental Information includes six figures and can be found with this article online at https://doi.org/10.1016/j.celrep.2017.12.036.

ACKNOWLEDGMENTS

This research was supported by the Howard Hughes Medical Institute (E.R.K.) and Cohen Veterans Bioscience (J.B.R. and E.R.K.).

AUTHOR CONTRIBUTIONS

J.B.R. conceived the study, designed and performed the experiments, analyzed the data, and wrote the manuscript. K.A.K. prepared recombinant proteins and helped perform experiments. E.R.K. helped prepare the manuscript and provided conceptual guidance.

DECLARATION OF INTERESTS

The authors declare no competing interests.

Received: September 8, 2017
Revised: November 8, 2017
Accepted: December 11, 2017
Published: January 2, 2018

REFERENCES

Anderson, P., and Kedersha, N. (2002). Visibly stressed: the role of eIF2, TIA-1, and stress granules in protein translation. Cell Stress Chaperones *7*, 213–221.

Anderson, P., and Kedersha, N. (2008). Stress granules: the Tao of RNA triage. Trends Biochem. Sci. *33*, 141–150.

Arimoto, K., Fukuda, H., Imajoh-Ohmi, S., Saito, H., and Takekawa, M. (2008). Formation of stress granules inhibits apoptosis by suppressing stress-responsive MAPK pathways. Nat. Cell Biol. *10*, 1324–1332.

Arimoto-Matsuzaki, K., Saito, H., and Takekawa, M. (2016). TIA1 oxidation inhibits stress granule assembly and sensitizes cells to stress-induced apoptosis. Nat. Commun. *7*, 10252.

Bley, N., Lederer, M., Pfalz, B., Reinke, C., Fuchs, T., Glaß, M., Möller, B., and Hüttelmaier, S. (2015). Stress granules are dispensable for mRNA stabilization during cellular stress. Nucleic Acids Res. *43*, e26.

Bounedjah, O., Desforges, B., Wu, T.D., Pioche-Durieu, C., Marco, S., Hamon, L., Curmi, P.A., Guerquin-Kern, J.L., Piétrement, O., and Pastré, D. (2014). Free mRNA in excess upon polysome dissociation is a scaffold for protein multimerization to form stress granules. Nucleic Acids Res. *42*, 8678–8691.

Buchan, J.R., and Parker, R. (2009). Eukaryotic stress granules: the ins and outs of translation. Mol. Cell *36*, 932–941.

Dean, K.M., Qin, Y., and Palmer, A.E. (2012). Visualizing metal ions in cells: an overview of analytical techniques, approaches, and probes. Biochim. Biophys. Acta *1823*, 1406–1415.

Diaz-Espinoza, R., and Soto, C. (2012). High-resolution structure of infectious prion protein: the final frontier. Nat. Struct. Mol. Biol. *19*, 370–377.

Dyson, H.J., and Wright, P.E. (2005). Intrinsically unstructured proteins and their functions. Nat. Rev. Mol. Cell Biol. *6*, 197–208.

Evers, T.H., Appelhof, M.A., Meijer, E.W., and Merkx, M. (2008). His-tags as Zn(II) binding motifs in a protein-based fluorescent sensor. Protein Eng. Des. Sel. *21*, 529–536.

Fioriti, L., Myers, C., Huang, Y.Y., Li, X., Stephan, J.S., Trifilieff, P., Colnaghi, L., Kosmidis, S., Drisaldi, B., Pavlopoulos, E., and Kandel, E.R. (2015). The persistence of hippocampal-based memory requires protein synthesis mediated by the prion-like protein CPEB3. Neuron *86*, 1433–1448.

Gilks, N., Kedersha, N., Ayodele, M., Shen, L., Stoecklin, G., Dember, L.M., and Anderson, P. (2004). Stress granule assembly is mediated by prion-like aggregation of TIA-1. Mol. Biol. Cell *15*, 5383–5398.

Hall, D.R., Gourley, D.G., Leonard, G.A., Duke, E.M., Anderson, L.A., Boxer, D.H., and Hunter, W.N. (1999). The high-resolution crystal structure of the molybdate-dependent transcriptional regulator (ModE) from *Escherichia coli*: a novel combination of domain folds. EMBO J. *18*, 1435–1446.

Hojyo, S., and Fukada, T. (2016). Roles of zinc signaling in the immune system. J. Immunol. Res. *2016*, 6762343.

Hou, F., Sun, L., Zheng, H., Skaug, B., Jiang, Q.X., and Chen, Z.J. (2011). MAVS forms functional prion-like aggregates to activate and propagate antiviral innate immune response. Cell *146*, 448–461.

Jain, S., Wheeler, J.R., Walters, R.W., Agrawal, A., Barsic, A., and Parker, R. (2016). ATPase-modulated stress granules contain a diverse proteome and substructure. Cell *164*, 487–498.

Jayabalan, A.K., Sanchez, A., Park, R.Y., Yoon, S.P., Kang, G.Y., Baek, J.H., Anderson, P., Kee, Y., and Ohn, T. (2016). NEDDylation promotes stress granule assembly. Nat. Commun. *7*, 12125.

Kato, M., Han, T.W., Xie, S., Shi, K., Du, X., Wu, L.C., Mirzaei, H., Goldsmith, E.J., Longgood, J., Pei, J., et al. (2012). Cell-free formation of RNA granules: low complexity sequence domains form dynamic fibers within hydrogels. Cell *149*, 753–767.

Kedersha, N., and Anderson, P. (2007). Mammalian stress granules and processing bodies. Methods Enzymol. *431*, 61–81.

Kedersha, N., Cho, M.R., Li, W., Yacono, P.W., Chen, S., Gilks, N., Golan, D.E., and Anderson, P. (2000). Dynamic shuttling of TIA-1 accompanies the recruitment of mRNA to mammalian stress granules. J. Cell Biol. *151*, 1257–1268.

Kedersha, N., Stoecklin, G., Ayodele, M., Yacono, P., Lykke-Andersen, J., Fritzler, M.J., Scheuner, D., Kaufman, R.J., Golan, D.E., and Anderson, P. (2005). Stress granules and processing bodies are dynamically linked sites of mRNP remodeling. J. Cell Biol. *169*, 871–884.

Kedersha, N., Tisdale, S., Hickman, T., and Anderson, P. (2008). Real-time and quantitative imaging of mammalian stress granules and processing bodies. Methods Enzymol. *448*, 521–552.

Kedersha, N., Ivanov, P., and Anderson, P. (2013). Stress granules and cell signaling: more than just a passing phase? Trends Biochem. Sci. *38*, 494–506.

Li, X., Rayman, J.B., Kandel, E.R., and Derkatch, I.L. (2014). Functional role of Tia1/Pub1 and Sup35 prion domains: directing protein synthesis machinery to the tubulin cytoskeleton. Mol. Cell *55*, 305–318.

Liang, X., Dempski, R.E., and Burdette, S.C. (2016). Zn(2+) at a cellular crossroads. Curr. Opin. Chem. Biol. *31*, 120–125.

Lin, Y., Protter, D.S., Rosen, M.K., and Parker, R. (2015). Formation and maturation of phase-separated liquid droplets by RNA-binding proteins. Mol. Cell *60*, 208–219.

Majumdar, A., Cesario, W.C., White-Grindley, E., Jiang, H., Ren, F., Khan, M.R., Li, L., Choi, E.M., Kannan, K., Guo, F., et al. (2012). Critical role of amyloid-like oligomers of *Drosophila* Orb2 in the persistence of memory. Cell *148*, 515–529.

Matheou, C.J., Younan, N.D., and Viles, J.H. (2016). The rapid exchange of zinc(2+) enables trace levels to profoundly influence amyloid-β misfolding and dominates assembly outcomes in Cu(2+)/Zn(2+) mixtures. J. Mol. Biol. *428*, 2832–2846.

McCormick, N., Velasquez, V., Finney, L., Vogt, S., and Kelleher, S.L. (2010). X-ray fluorescence microscopy reveals accumulation and secretion of discrete intracellular zinc pools in the lactating mouse mammary gland. PLoS ONE *5*, e11078.

Micsonai, A., Wien, F., Kernya, L., Lee, Y.H., Goto, Y., Réfrégiers, M., and Kardos, J. (2015). Accurate secondary structure prediction and fold recognition for circular dichroism spectroscopy. Proc. Natl. Acad. Sci. USA *112*, E3095–E3103.

Muylle, F.A., Adriaensen, D., De Coen, W., Timmermans, J.P., and Blust, R. (2006). Tracing of labile zinc in live fish hepatocytes using FluoZin-3. Biometals *19*, 437–450.

Nott, T.J., Petsalaki, E., Farber, P., Jervis, D., Fussner, E., Plochowietz, A., Craggs, T.D., Bazett-Jones, D.P., Pawson, T., Forman-Kay, J.D., and Baldwin, A.J. (2015). Phase transition of a disordered nuage protein generates environmentally responsive membraneless organelles. Mol. Cell *57*, 936–947.

Ohn, T., Kedersha, N., Hickman, T., Tisdale, S., and Anderson, P. (2008). A functional RNAi screen links O-GlcNAc modification of ribosomal proteins to stress granule and processing body assembly. Nat. Cell Biol. *10*, 1224–1231.

Ohshima, D., Arimoto-Matsuzaki, K., Tomida, T., Takekawa, M., and Ichikawa, K. (2015). Spatio-temporal dynamics and mechanisms of stress granule assembly. PLoS Comput. Biol. *11*, e1004326.

Oteiza, P.I. (2012). Zinc and the modulation of redox homeostasis. Free Radic. Biol. Med. *53*, 1748–1759.

Pan, K.M., Baldwin, M., Nguyen, J., Gasset, M., Serban, A., Groth, D., Mehlhorn, I., Huang, Z., Fletterick, R.J., Cohen, F.E., et al. (1993). Conversion of alpha-helices into beta-sheets features in the formation of the scrapie prion proteins. Proc. Natl. Acad. Sci. USA *90*, 10962–10966.

Pan, K., Yi, C.W., Chen, J., and Liang, Y. (2015). Zinc significantly changes the aggregation pathway and the conformation of aggregates of human prion protein. Biochim. Biophys. Acta *1854*, 907–918.

Protter, D.S., and Parker, R. (2016). Principles and properties of stress granules. Trends Cell Biol. *26*, 668–679.

Rayman, J.B., and Kandel, E.R. (2017a). Functional prions in the brain. Cold Spring Harb. Perspect. Biol. *9*, a023671.

Rayman, J.B., and Kandel, E.R. (2017b). TIA-1 is a functional prion-like protein. Cold Spring Harb. Perspect. Biol. *9*, a030718.

Schuh, R.A., Clerc, P., Hwang, H., Mehrabian, Z., Bittman, K., Chen, H., and Polster, B.M. (2011). Adaptation of microplate-based respirometry for hippocampal slices and analysis of respiratory capacity. J. Neurosci. Res. *89*, 1979–1988.

Shin, Y., and Brangwynne, C.P. (2017). Liquid phase condensation in cell physiology and disease. Science *357*, eaaf4382.

Si, K., Lindquist, S., and Kandel, E.R. (2003). A neuronal isoform of the aplysia CPEB has prion-like properties. Cell *115*, 879–891.

Stephan, J.S., Fioriti, L., Lamba, N., Colnaghi, L., Karl, K., Derkatch, I.L., and Kandel, E.R. (2015). The CPEB3 protein is a functional prion that interacts with the actin cytoskeleton. Cell Rep. *11*, 1772–1785.

Takeda, A., Fujii, H., Minamino, T., and Tamano, H. (2014). Intracellular Zn(2+) signaling in cognition. J. Neurosci. Res. *92*, 819–824.

Tourrière, H., Chebli, K., Zekri, L., Courselaud, B., Blanchard, J.M., Bertrand, E., and Tazi, J. (2003). The RasGAP-associated endoribonuclease G3BP assembles stress granules. J. Cell Biol. *160*, 823–831.

Wippich, F., Bodenmiller, B., Trajkovska, M.G., Wanka, S., Aebersold, R., and Pelkmans, L. (2013). Dual specificity kinase DYRK3 couples stress granule condensation/dissolution to mTORC1 signaling. Cell *152*, 791–805.

Yamasaki, S., Sakata-Sogawa, K., Hasegawa, A., Suzuki, T., Kabu, K., Sato, E., Kurosaki, T., Yamashita, S., Tokunaga, M., Nishida, K., and Hirano, T. (2007). Zinc is a novel intracellular second messenger. J. Cell Biol. *177*, 637–645.